The Astrophysical Journal, 910:56 (10pp), 2021 March 20 https://doi.org/10.3847/1538-4357/abe45c

Mass–Velocity Dispersion Relation in HIFLUGCS Galaxy Clusters

Yong Tian[1], Po-Chieh Yu[2], Pengfei Li[3], Stacy S. McGaugh[3,5], and Chung-Ming Ko[1,4]
[1] Institute of Astronomy, National Central University, Taoyuan 32001, Taiwan; cmko@astro.ncu.edu.tw
[2] College of General Studies, Yuan-Ze University, Taoyuan 32003, Taiwan
[3] Department of Astronomy, Case Western Reserve University, Cleveland, OH 44106, USA; stacy.mcgaugh@case.edu
[4] Department of Physics and Center for Complex Systems, National Central University, Taoyuan 32001, Taiwan
Received 2020 October 1; revised 2021 January 29; accepted 2021 February 7; published 2021 March 25

Abstract

We investigate the mass–velocity dispersion relation (MVDR) in 29 galaxy clusters in the HIghest X-ray FLUx Galaxy Cluster Sample (HIFLUGCS). We measure the spatially resolved, line-of-sight velocity dispersion profiles of these clusters, which we find to be mostly flat at large radii, reminiscent of the rotation curves of galaxies. We discover a tight empirical relation between the baryonic mass $M_{\rm bar}$ and the flat velocity dispersion σ of the member galaxies, i.e., MVDR, $\log(M_{\rm bar}/M_\odot) = 4.1^{+0.4}_{-0.4}\log(\sigma/{\rm km\,s^{-1}}) + 1.6^{+1.0}_{-1.3}$, with the lognormal intrinsic scatter of 12^{+3}_{-3}%. The residuals of the MVDR are uncorrelated with other cluster properties like temperature, cluster radius, baryonic mass surface density, and redshift. These characteristics are reminiscent of the MVDR for individual galaxies, albeit at about a ten times larger characteristic acceleration scale. The cluster baryon fraction falls short of the cosmic value, exposing a problem: the discrepancy increases systematically for clusters of lower mass and lower baryonic acceleration.

Unified Astronomy Thesaurus concepts: Dark matter (353); Galaxy clusters (584); Galaxy groups (597); Intracluster medium (858); X-ray astronomy (1810)

1. Introduction

Kinematic scaling relations provide key tests and hints in understanding the dark matter problem. For example, Tully & Fisher (1977) found a relation between galactic luminosity and H I line widths. Later on, the baryonic Tully–Fisher relation (BTFR), $M_{\rm bar}\propto v^4$, was revealed as a tight relation in spiral galaxies (McGaugh et al. 2000; Verheijen 2001; McGaugh 2011; Lelli et al. 2016, 2019). Similarly, the mass–velocity dispersion relation (MVDR), $M_{\rm bar}\propto\sigma^4$, was expected in pressure-supported systems such as galaxy clusters and elliptical galaxies, and is also known as the Baryonic Faber–Jackson Relation (BFJR, Faber & Jackson 1976; Sanders 2010; Catinella et al. 2012; Cappellari et al. 2013; Aquino-Ortíz et al. 2018; Barat et al. 2019). These tight relations raise the critical issue of how the stochastic processes of galaxy formation can produce regularity in a Λ cold dark matter (ΛCDM) model by adapting the abundance matching relation (Dutton et al. 2010; Desmond & Wechsler 2015, 2017; Wechsler & Tinker 2018; Katz et al. 2019). By contrast, MOdified Newtonian Dynamics (MOND) directly implied these relations in its framework (Milgrom 1983; Sanders & McGaugh 2002; Famaey & McGaugh 2012).

Analogous to Kepler's and Newton's laws, the kinematic scaling relations, e.g., BTFR and BFJR, are the counterparts of the effective dynamical relations. For instance, in galactic systems, both relations can be implied by the low acceleration limit of the radial acceleration relation (RAR, McGaugh et al. 2016). The RAR is a tight relation between two independent measurements: the observed radial acceleration, $g_{\rm obs}=|\partial\Phi_{\rm tot}/\partial r|=v^2/r$, and the baryonic acceleration, $g_{\rm bar}=GM_{\rm bar}(<r)/r^2$, where $\Phi_{\rm tot}$ is the total gravitational potential and $M_{\rm bar}(<r)$ is the enclosed baryonic mass within the radius r. The low acceleration limit of the RAR gives $g_{\rm obs}\simeq\sqrt{g_{\rm bar}g_\dagger}$ with the acceleration scale $g_\dagger=(1.20\pm0.02)\times10^{-10}$ m s^{-2} (McGaugh et al. 2016, 2018; Lelli et al. 2017; Li et al. 2018). It incorporates $v_\infty^4=GM_{\rm bar}g_\dagger$ (BTFR) as well as $\sigma^4\propto GM_{\rm bar}g_\dagger$ (BFJR). In addition, the RAR is also confirmed in elliptical galaxies (Lelli et al. 2017; Tian & Ko 2017, 2019; Rong et al. 2018; Chae et al. 2019). As one interpretation of the RAR, MOND predicted the BTFR and the BFJR almost four decades ago (Milgrom 1983).

Given the tight scaling relations in galactic systems, it would be interesting to investigate them in the largest gravitationally bound systems, clusters of galaxies. The baryonic mass of a galaxy cluster includes the hot intracluster medium (ICM) and member galaxies. Due to the strong gravitational potential of the cluster, the ICM is mainly composed of ionized gases, which emits X-ray radiation mostly through the bremsstrahlung process (Lea et al. 1973). However, the luminous mass of a galaxy cluster is not enough to account for its gravity, as revealed by dynamical studies (Zwicky 1933; Bahcall 1977; Kravtsov & Borgani 2012; Overzier 2016; Rines et al. 2016) and gravitational lensing (Kneib & Natarajan 2011; Umetsu 2020). The discrepancy is considerably large, so MOND, although it predicts stronger dynamical effects at low accelerations, still presents a residual missing mass in galaxy clusters (Sanders 1999, 2003; Pointecouteau & Silk 2005; Famaey & McGaugh 2012; Tian et al. 2020). This indicates that the RAR must be different at the cluster scale.

More recently, Tian et al. (2020) studied 20 galaxy clusters from the Cluster Lensing And Supernova survey with Hubble (CLASH, Postman et al. 2012), and found a tight correlation between $g_{\rm obs}$ and $g_{\rm bar}$,

$$g_{\rm obs}\simeq\sqrt{g_{\rm bar}g_\ddagger}, \tag{1}$$

with a new acceleration scale $g_\ddagger=(2.0\pm0.1)\times10^{-9}$ m s^{-2}. In the CLASH RAR, $g_{\rm obs}$ is probed by strong-lensing, weak-lensing shear-and-magnification data (Umetsu et al. 2016), while $g_{\rm bar}$ is estimated by the distribution of X-ray gas mass

[5] Author to whom any correspondence should be addressed.

(Donahue et al. 2014) and stellar mass (Chiu et al. 2018). This tight relation is in contradiction to Chan & Del Popolo (2020), who claimed no such relation at the cluster scale. If the validity of the CLASH RAR is extended from gravitational lensing to dynamics, it will imply an MVDR in the galaxy cluster, i.e., $\sigma^4 \propto GM_{\rm bar}g_\ddagger$, with a new acceleration scale $g_\ddagger$ (see Section 4.3 in Tian et al. 2020).

In galaxy clusters, measurements of the MVDR were indirectly made by the study of the relation between the X-ray gas mass $M_{\rm gas}$ and the temperature T, $M_{\rm gas}-T$ (Sanders 1994; Ettori et al. 2004; Angus et al. 2008; Famaey & McGaugh 2012). Sanders (1994) first found a rough correlation of $M_{\rm gas} \propto T^2$ for 20 rich galaxy clusters. Famaey & McGaugh (2012) obtained a similar result by combining rich clusters (Reiprich & Böhringer 2002; Sanders 2003) and galaxy groups (Angus et al. 2008). Their results indicated a slope consistent with $M_{\rm gas} \propto T^2$ predicted by MOND, but not a consistent normalization factor. By contrast, this slope deviated from the conventional prediction of $M_{\rm gas} \propto T^{2/3}$ in the ΛCDM paradigm (Famaey & McGaugh 2012; McGaugh 2015).

In the literature, the MVDR has never been clearly quantified in galaxy clusters. Some studies focus on the X-ray luminosity–velocity dispersion relation (e.g., Mulchaey & Zabludoff 1998; Xue & Wu 2000; Mahdavi & Geller 2001; Popesso et al. 2005; Zhang et al. 2011), as both quantities are directly measured. To convert $M-T$ into $M-\sigma$ requires an additional scaling relation $T-\sigma$, with both $M_{\rm gas}$ and T depending on X-ray observations. The normalization of the intercept implies a different acceleration scale in galaxy clusters (Famaey & McGaugh 2012). However, this new scale has never been estimated numerically. That said, Milgrom (2019) found the acceleration scale in intermediate-richness galaxy groups is consistent with MOND.

In this work, we investigate the MVDR by directly studying the baryonic mass of clusters and the velocity dispersion of member galaxies in 29 HIFLUGCS clusters. The paper is organized as follows. In Section 2, we describe the properties of the sample and the methods to the velocity dispersion. In Section 3, we analyze the MVDR by Bayesian statistics and present the residuals versus other cluster properties. In Section 4, we compare our result with the CLASH RAR, test it on the dark matter model, and estimate the baryon fraction against the baryonic mass and the baryonic acceleration. Throughout this paper, we assume a flat ΛCDM cosmology with $\Omega_{\rm m}=0.3$, $\Omega_\Lambda=0.7$, and a Hubble constant of $H_0=70$ km s^{-1} Mpc^{-1}, in order to be consistent with the measurement in the HIFLUGCS.

2. Data and Methods

Studying the MVDR of galaxy clusters needs measures of both the baryonic mass and the velocity dispersion. The majority of the baryonic mass is dominated by the X-ray gas mass due to the strong gravitational potential of the clusters. In hydrostatic equilibrium, the velocity dispersion of member galaxies can represent the kinematics of a whole cluster.

The analysis of the velocity dispersion requires the relative line-of-sight (los) velocity of member galaxies to the cluster center. In the CLASH RAR, the cluster center is found to be the brightest cluster galaxy (BCG) in the CLASH sample (Umetsu et al. 2014, 2016). BCGs are usually positioned at the geometric and kinematic center of the cluster, the central peak of the X-ray emission (Jones & Forman 1984; Lin & Mohr 2004), and the minimum of the gravitational potential well (Zitrin et al. 2012). Because of the MVDR implied by the CLASH RAR, a consistent result needs to adopt the BCG as the cluster center.

For our study, an appropriate cluster database should provide a wide variety of the X-ray gas mass and optical measurements of BCGs and member galaxies, and the analysis of an offset between the BCG position and the X-ray flux-weighted cluster center. To satisfy these requirements, we used the HIFLUGCS (Reiprich & Böhringer 2002), which contained 64 galaxy clusters selected from the ROSAT All-Sky Survey (Ebeling et al. 1998; Böhringer et al. 2000, 2004). The X-ray measurement of 63 galaxy clusters was refined by combing through the excellent quality X-ray data in the XMM-Newton archive (Zhang et al. 2011). In addition, Zhang et al. (2011) collected member galaxies and analyzed the offset of clusters center.

In this work, we focus on a subset of 29 clusters in the HIFLUGCS constrained by the cluster center offset and the information about member galaxies. The median of the offset in 61 HIFLUGCS clusters is 12 kpc, ranging from 0.4 kpc to 955 kpc. Since a typical BCG effective radius is $\approx$30 kpc (Schneider et al. 1983; Schombert 1986; Tian et al. 2020), we restrict the cluster center offset to within 60 kpc, which narrows the sample down to 51 galaxy clusters. It is relatively small compared to the average HIFLUGCS cluster radius, $r_{500}\approx 1$ Mpc, at which the mass density is 500 times the critical density. Among these, only 29 clusters have the required information about member galaxies in the literature. The properties of 29 BCGs and clusters are listed in Tables 1 and 2, respectively.

2.1. Baryonic Mass

The baryonic mass $M_{\rm bar}$ of galaxy clusters comprises the X-ray gas mass $M_{\rm gas}$ as the major component and the stellar mass $M_{\rm star}$ as a minor one. Most baryons in clusters are in the form of ionized gas that emits X-rays due to the strong gravitational potential of clusters. The subdominant component includes the stellar mass of BCGs and all member galaxies.

Zhang et al. (2011) found 63 clusters in the HIFLUGCS available in the XMM-Newton archive. They analyzed ∼1.3 Ms XMM-Newton data for 57 clusters, excluding four flared clusters and two with multiple redshifts. The X-ray gas mass was estimated within r_{500} by combining both XMM-Newton and ROSAT X-ray data. In our subset of HIFLUGCS clusters, the X-ray gas mass ranges from $1.7\times10^{11}\,M_\odot$ to $1.3\times10^{14}\,M_\odot$, and are listed in Table 2.

Apart from the dominant component of the X-ray gas mass, the total baryonic mass still needs the small contribution of the stellar mass. The fraction between the stellar mass and the baryonic mass, $f_{\rm star}(r)\equiv M_{\rm star}(<r)/M_{\rm gas}(<r)$, depends on gas mass and radius. For a large cluster with the typical X-ray gas mass $\sim5\times10^{14}\,M_\odot$, it is negligible (∼6%) at one megaparsec (Chiu et al. 2018), which is the average HIFLUGCS cluster radius of r_{500} in our subsample. However, this fraction increases toward lower gas mass. For example, Kravtsov & Borgani (2012) found it around 5–20% at r_{500}, corresponding to a range of $M_{\rm gas}$ of 10^{14}–$10^{13}\,M_\odot$.

We estimated the stellar mass by the scaling relation of the fraction $f_{\rm star}$ at r_{500} (e.g., see Equation (11) in Giodini et al. 2009). With 91 COSMOS X-ray selected clusters and 27

Table 1
Properties of 29 HIFLUGCS BCGs

Name	z	R.A. (J2000.0)	Decl. (J2000.0)	V_{los}[a] (km s^{-1})
NGC 4636	0.0031	12:42:49.87	+02:41:16.01	919
Fornax	0.0048	03:38:29.00	−35:27:02.67	1422
A3526	0.0097	12:48:49.28	−41:18:39.92	2904
A1060	0.0130	10:36:42.82	−27:31:42.02	3858
A262	0.0162	01:52:46.48	+36:09:06.53	4823
A3581	0.0220	14:07:29.50	−27:01:07.00	6531
A4038	0.0291	23:47:45.11	−28:08:26.67	8605
A2634	0.0314	23:40:00.84	+27:08:01.37	9256
A496	0.0327	04:33:37.84	−13:15:43.04	9651
A2063	0.0341	15:23:05.30	+08:36:33.18	10,055
A2052	0.0350	15:16:44.50	+07:01:17.00	10,314
A2147	0.0354	16:02:17.00	+15:58:28.25	10,419
A576	0.0381	07:21:30.24	+55:45:41.69	11,200
A3571	0.0386	13:47:28.39	−32:51:54.02	11,353
A2589	0.0412	23:23:57.41	+16:46:37.94	12,088
A2657	0.0421	23:44:57.42	+09:11:35.39	12,361
A119	0.0446	00:56:16.10	−01:15:19.77	13,080
A3558	0.0470	13:27:56.88	−31:29:43.71	13,762
A1644	0.0488	12:57:11.58	−17:24:34.47	14,267
A3562	0.0502	13:33:34.74	−31:40:20.16	14,677
A4059	0.0504	23:57:00.40	−34:45:32.00	14,740
A3391	0.0552	06:26:20.45	−53:41:35.89	16,102
A85	0.0554	00:41:50.45	−09:18:11.46	16,138
A133	0.0560	01:02:41.77	−21:52:55.75	16,314
A3158	0.0581	03:42:52.95	−53:37:52.69	16,899
A3266	0.0610	04:31:13.31	−61:27:11.43	17,724
A1795	0.0613	13:47:22.56	+26:22:51.91	17,815
A2029	0.0779	15:10:56.10	+05:44:41.19	22,447
A2142	0.0908	15:58:20.03	+27:14:00.06	25,993

Note.
[a] The los velocity of the BCG.

nearby X-ray clusters, Giodini et al. (2009) found

$$f_{\rm star} = (5.0^{+0.1}_{-0.1}) \times 10^{-2}\left(\frac{M_{\rm gas}}{5 \times 10^{13} M_{\odot}}\right)^{-0.37^{+0.04}_{-0.04}}. \quad (2)$$

According to this relation, the median of $f_{\rm star}$ is 7% for our sample. However, it is significant for the two smallest clusters: Fornax ($f_{\rm star} = 27\%$) and the NGC 4636 group ($f_{\rm star} = 41\%$). Therefore, we obtain the baryonic mass of 29 HIFLUGCS clusters as well as their uncertainties, as listed in Table 2.

2.2. Velocity Dispersion

Implied by the CLASH RAR, the flat velocity dispersion of the cluster in the tail is correlated with the total baryonic mass for the MVDR. Assuming hydrostatic equilibrium, member galaxies are the tracers of the gravitational potential in the galaxy clusters. We can study the los velocity of the member galaxies to get a flat velocity dispersion of the cluster by treating the BCG as the cluster center.

2.2.1. BCGs and Member Galaxies

We collected BCGs and member galaxies from the literature, the sample of which was organized and identified by the probability of membership in SIMBAD[6] (Wenger et al. 2000). We carefully excluded uncertain members as well as incomplete optical data of galaxies. As the memberships were identified by multiple references, we eliminated the repeated members. Information about the BCGs and member galaxies include the position, los velocity, and redshift. Three examples (A85, A262, and Fornax) of the two-dimensional distributions are shown in the upper panel of Figure 1.

By requiring more than 30 member galaxies, we have a subsample of 29 clusters in the HIFLUGCS besides the A2199 supercluster. In total, there are 4926 member galaxies in our sample, which gives 170 members per cluster on average. Among these, we excluded the A2199 supercluster because of its complexity of multiple BCGs and clusters (Lee et al. 2015). Finally, all available candidates remain within the 29 galaxy clusters in our study.

Most clusters in the HIFLUGCS have a single BCG in their center, but some have a dumbbell, a pair of BCGs, or even multiple nuclei (A2199). However, Zhang et al. (2011) reported 13 HIFLUGCS clusters with more than one BCG. In those cases, the BCG position is considered to be at the brighter one or at the center of the dumbbell. In our sample, five of them (A576, A2634, A3158, A3266, and A3391) have dumbbell BCGs. We chose either one of them as the cluster center.

In our sample, most of the member galaxies are identified by the optical measurement. However, besides 234 members from the optical measurement in galaxy group NGC 4636 (referred to as the M31 group), 12 members are determined by using H I measurements (Kilborn et al. 2009). In the velocity distribution diagram, these 12 members form a separate group from the other 234 members. In addition, the relative los velocity of them is systematically deviated from the BCG. Thus, we excluded these 12 galaxies from the membership of the NGC 4636 group.

2.2.2. Methods

The process of estimating the velocity dispersion of a galaxy cluster is similar to that for an elliptical galaxy, i.e., to treat a cluster as a galaxy and member galaxies as stars. With the BCG as the center, we computed the relative projected radius and relative los velocity for each member galaxy; see three examples in the lower panel of Figure 1. In our sample, the BCGs are sitting at the geometric and kinematic center, which justifies our requirements.

Because the velocity dispersion measured within larger radii better represents the total kinetic energy, we calculate them by the binned data of the member galaxies. For each bin, the histogram presents a Gaussian distribution in the velocity profile. The los velocity dispersion is evaluated by the half Gaussian width of the relative los velocity profile. We also analyzed the error of the los velocity dispersion. All 29 clusters show a flat velocity dispersion in the tail. We adopted the last bin for the los velocity dispersion, which is listed in Table 2.

To evaluate non-Gaussian effects, we implement the biweight estimator (Beers et al. 1990) as an independent, statistically robust method to determine the velocity dispersion. The biweight scale for the last binned data point yields highly consistent results. Because the last binned data are presented as the Gaussian distribution, the biweight scale asymptotically approaches the Gaussian method.

We compare our results with the total velocity dispersion reported by Zhang et al. (2011). We found no distinguishable

[6] http://simbad.u-strasbg.fr/simbad/

Table 2
Properties of 29 HIFLUGCS Clusters

Name	D[a] (Mpc)	r_{500}[b] (kpc)	kT_{vir}[c] (kpc)	$\log(M_{gas})$[d] ($M_\odot$)	$\log(M_{bar})$[e] ($M_\odot$)	σ_{last}[f] (km s^{-1})	r_{last}[g] (kpc)	N_{gal}[h]	Reference
NGC 4636	13	255	0.9	11.230 ± 0.059	11.379 ± 0.056	229 ± 21	29 ± 7	234	28,29,30
Fornax	20	250	1.3	11.724 ± 0.006	11.827 ± 0.018	252 ± 36	1384 ± 313	68	31,32
A3526	41	761	3.9	13.037 ± 0.040	13.074 ± 0.037	890 ± 110	779 ± 509	97	3,11,12,13,18,26,27
A1060	55	714	3.2	12.934 ± 0.048	12.974 ± 0.044	634 ± 65	389 ± 359	186	3,11,12,13,14,15
A262	68	755	2.4	13.033 ± 0.048	13.070 ± 0.044	551 ± 68	2125 ± 995	95	3,11,12,13,33,34
A3581	92	606	2.0	12.708 ± 0.050	12.756 ± 0.045	436 ± 77	649 ± 520	32	3,11,12,18,19,20,35,36
A4038	120	858	3.1	13.253 ± 0.034	13.284 ± 0.032	773 ± 125	513 ± 128	53	3,11,13,18
A2634	129	789	3.2	13.140 ± 0.028	13.174 ± 0.026	731 ± 103	1220 ± 340	73	3,11,13
A496	135	967	4.9	13.446 ± 0.019	13.472 ± 0.018	648 ± 71	805 ± 161	126	3,8,10
A2063	140	874	3.8	13.301 ± 0.020	13.330 ± 0.019	779 ± 120	844 ± 311	63	3,9,11,18,20
A2052	144	857	3.4	13.290 ± 0.024	13.320 ± 0.023	475 ± 61	622 ± 157	59	3,9,18,19
A2147	145	1057	4.1	13.592 ± 0.044	13.615 ± 0.042	811 ± 106	1146 ± 177	87	3,8,9
A576	156	869	4.1	13.301 ± 0.154	13.330 ± 0.144	923 ± 126	1582 ± 411	79	3,11,12,18,19,36
A3571	158	1133	7.0	13.713 ± 0.024	13.734 ± 0.023	841 ± 84	999 ± 536	99	3,11,18
A2589	168	837	3.9	13.248 ± 0.029	13.279 ± 0.027	610 ± 83	1148 ± 225	77	1,3,7,8,23
A2657	171	820	3.5	13.215 ± 0.019	13.247 ± 0.018	789 ± 131	666 ± 214	35	3,17,18
A119	181	1062	5.7	13.630 ± 0.020	13.652 ± 0.019	648 ± 51	1240 ± 316	240	3,6,7,8,9
A3558	190	1188	5.0	13.806 ± 0.013	13.825 ± 0.012	820 ± 86	1558 ± 781	138	1,3,11,12,27
A1644	197	1077	5.1	13.626 ± 0.063	13.649 ± 0.060	901 ± 86	1060 ± 120	211	1,3,7,19,37
A3562	202	904	4.4	13.377 ± 0.016	13.405 ± 0.015	729 ± 129	1269 ± 267	48	3,8,27
A4059	203	892	4.2	13.350 ± 0.033	13.378 ± 0.031	666 ± 94	926 ± 301	50	1,3,8,19
A3391	221	971	5.8	13.500 ± 0.026	13.525 ± 0.025	885 ± 152	1815 ± 511	49	3,19
A85	222	1217	6.0	13.824 ± 0.021	13.843 ± 0.020	934 ± 74	1536 ± 300	465	1,2,3,4,5
A133	224	885	4.0	13.364 ± 0.019	13.392 ± 0.018	803 ± 147	1021 ± 191	45	1,3
A3158	232	1013	5.0	13.574 ± 0.038	13.598 ± 0.036	985 ± 83	1581 ± 340	206	1,3,7
A3266	243	1265	9.5	13.924 ± 0.020	13.942 ± 0.019	1226 ± 95	2848 ± 868	327	1,3,7,24,25
A1795	244	1085	6.1	13.695 ± 0.012	13.716 ± 0.011	831 ± 99	3087 ± 488	105	1,3,7,9
A2029	304	1247	8.3	13.916 ± 0.015	13.934 ± 0.014	844 ± 41	2751 ± 404	1056	16,17,38,39
A2142	349	1371	8.4	14.127 ± 0.003	14.142 ± 0.003	1062 ± 70	3012 ± 131	994	9,21,22

Notes.
[a] The angular diameter distance with the cluster center taken to be the position of the BCG.
[b] The cluster radius in Zhang et al. (2011).
[c] The cluster viral temperature in Hudson et al. (2010).
[d] The X-ray gas mass of the galaxy cluster within r_{500} in Zhang et al. (2011).
[e] The baryonic mass of the galaxy cluster within r_{500}, including the stellar mass estimated by the scaling relation in Giodini et al. (2009).
[f] The los velocity dispersion at the last binned point.
[g] The projected radius of the last binned point.
[h] The number of member galaxies.
References. (1) Poggianti et al. (2016), (2) Agulli et al. (2016), (3) Smith et al. (2004), (4) Arnold et al. (2009), (5) Fogarty et al. (2015), (6) Tian et al. (2012), (7) Cava et al. (2009), (8) Laine et al. (2003), (9) Szabo et al. (2011), (10) Chilingarian et al. (2008), (11) Hudson et al. (2001), (12) Smith et al. (2001), (13) Faber et al. (1989), (14) Misgeld et al. (2008), (15) Misgeld et al. (2011), (16) Tyler et al. (2013), (17) Rafferty et al. (2008), (18) Smith et al. (2000), (19) Lauer et al. (2014), (20) Coziol et al. (2009), (21) Owers et al. (2011), (22) Von Der Linden et al. (2007), (23) Liu et al. (2011), (24) Bai et al. (2009), (25) Dehghan et al. (2017), (26) Chiboucas & Mateo (2006), (27) Chilingarian et al. (2009), (28) Kilborn et al. (2009), (29) Park et al. (2010), (30) Schuberth et al. (2006), (31) Ferguson (1989), (32) Ferguson & Sandage (1990), (33) Thomas et al. (2008), (34) Sakai et al. (2012), (35) Guzzo et al. (2009), (36) Hoffer et al. (2012), (37) Marziani et al. (2017), (38) Sohn et al. (2017), and (39) Jørgensen et al. (2018).

differences in the total velocity dispersions except for A3526, which is estimated as 890 km s^{-1} instead of 486 km s^{-1} (Table 1 in Zhang et al. 2011). Without their data set of member galaxies, we cannot check this discrepancy further. Despite that, our calculation is more reasonable because the velocity dispersion is expected to be proportional to the X-ray gas mass. As for the flat tail, half of them are almost identical to the total velocity dispersion. The rest of them are ~10% smaller than the total value. This discovery is also similar to theirs.

3. Results

Our main goal is to explore the empirical kinematic scaling relation between two independent measurements: the baryonic mass of galaxy clusters and the flat los velocity dispersion of the member galaxies, i.e., the MVDR. To understand the tightness of the relation and the correlations among the cluster properties, we also study the intrinsic scatter and the residuals with Bayesian statistics. The relation and the residuals are presented in the following subsections.

3.1. MVDR with Bayesian Statistics

In the logarithmic plane of the MVDR, 29 HIFLUGCS clusters are distributed as a linear relation. We model it by $y = mx + b$ with two independent variables: $y \equiv \ln(M_{bar}/M_\odot)$ and $x \equiv \ln(\sigma_{los}/\mathrm{km\ s^{-1}})$. With Bayesian statistics, we adopt the orthogonal-distance-regression (ODR) method with a Markov Chain Monte Carlo (MCMC) analysis in Lelli et al. (2019). The ODR method is reasonable as two criteria are

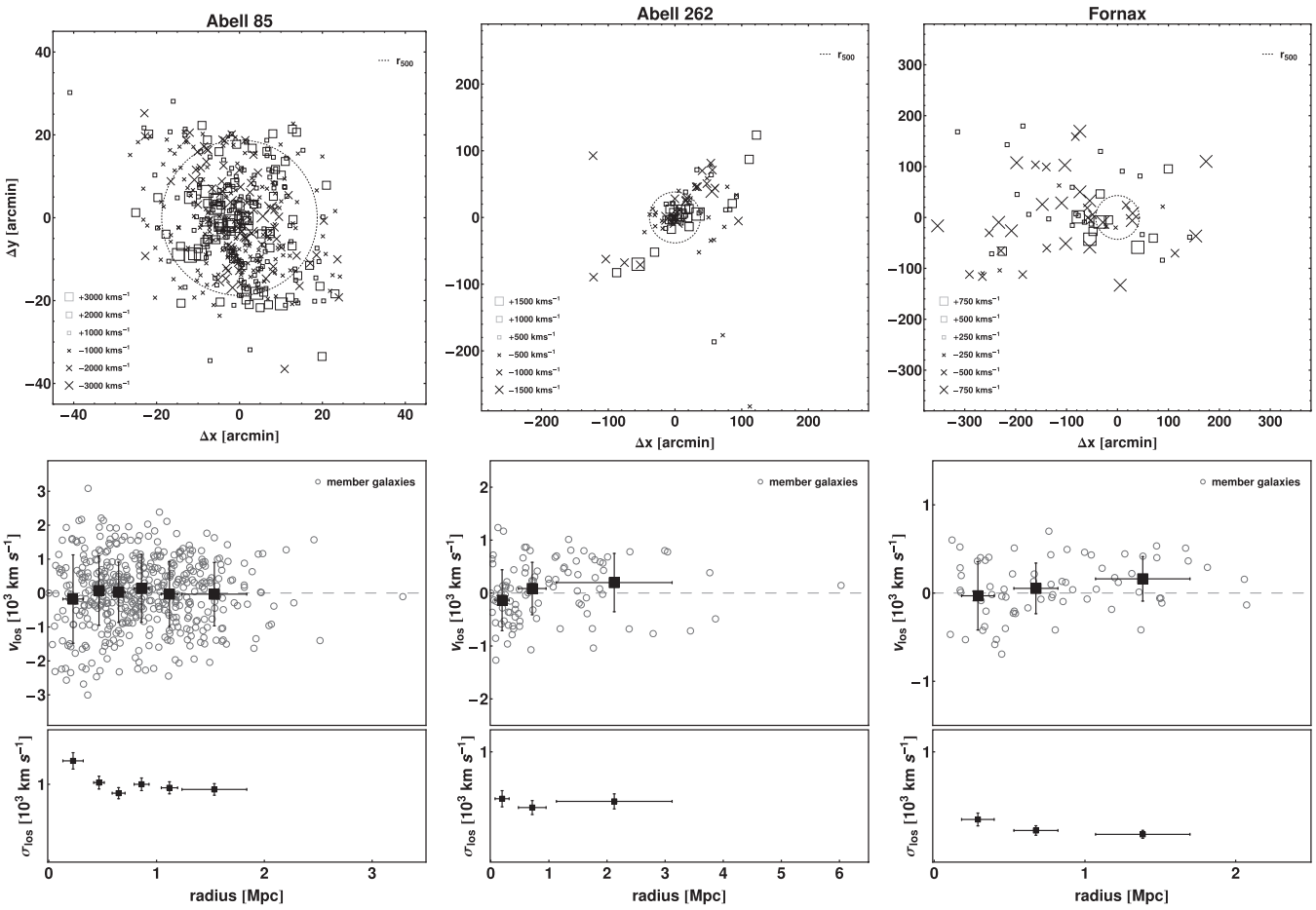

Figure 1. Three examples (A85, A262, and Fornax) of the 29 HUFLUGCS clusters. A85 is the most massive among the three, while Fornax is the least massive. Upper panel: the spatial distributions and the los velocity of member galaxies are relative to the center point of the BCG. The symbol sizes are proportional to the velocity magnitudes. Crosses indicate receding velocities; boxes, approaching velocities; dotted circles, r_{500}. Middle panel: the relative los velocity ($V_{\rm los}$) distribution is in terms of the projected radius relative to the BCG. The black filled rectangles represent the mean of the relative los velocity in each bin. The los velocity dispersion ($\sigma_{\rm los}$) is the vertical standard deviation of the binned data. Lower panel: the los velocity dispersion ($\sigma_{\rm los}$) presents a flat tail for each cluster.

satisfied: (1) a Gaussian intrinsic scatter perpendicular to the fitting line; (2) two independent errors of the x-axis σ_{x_i} and y-axis σ_{y_i}.

The log-likelihood function is written as

$$-2\ln\mathcal{L} = \sum_i \ln(2\pi\sigma_i^2) + \sum_i \frac{\Delta_i^2}{\sigma_i^2}, \tag{3}$$

with

$$\Delta_i^2 = \frac{(y_i - m\,x_i - b)^2}{m^2+1}, \tag{4}$$

where i runs over all data points, and σ_i includes the observational uncertainties (σ_{x_i}, σ_{y_i}) and the lognormal intrinsic scatter $\sigma_{\rm int}$ (e.g., see Appendix A in Lelli et al. 2019),

$$\sigma_i^2 = \frac{m^2\sigma_{x_i}^2}{m^2+1} + \frac{\sigma_{y_i}^2}{m^2+1} + \sigma_{\rm int}^2. \tag{5}$$

We implement the MCMC analysis for the slope and the intercept of the MVDR by EMCEE (Foreman-Mackey et al. 2013, 2019). We use noninformative flat priors on the slope m and the intercept b within the interval of $[-100, 100]$, and the intrinsic scatter $\ln\sigma_{\rm int} \in [-5, 2]$; see the result in Figure 2. It gives a relation as

$$\log\left(\frac{M_{\rm bar}}{M_\odot}\right) = 4.1^{+0.4}_{-0.4}\log\left(\frac{\sigma_{\rm los}}{\rm km\ s^{-1}}\right) + 1.6^{+1.0}_{-1.3}, \tag{6}$$

which is a tight relation with the error budget of the lognormal intrinsic scatter of 12^{+3}_{-3}%. Our result is consistent with the CLASH RAR, which implies $M_{\rm bar}\propto\sigma^4$.

To justify the initial assumption of a Gaussian intrinsic scatter perpendicular to the fitting line, we examine the histogram of the orthogonal residuals Δ_i with respect to Equation (6); (see the inset panel of Figure 2). The distributions of the residuals presents a Gaussian distribution with a tiny half width (0.07 dex).

To compare the new acceleration scale $g_\ddagger$ with Equation (1), the slope must be fixed to four. This scale $g_\ddagger$ depends on the intercept, which is highly sensitive to the slope; see the posterior distributions of the fitting parameters in Figure 2. In addition, the correct unit of the acceleration scale demands that the slope be exactly four. We perform the MCMC analysis again to get

$$\log\left(\frac{M_{\rm bar}}{M_\odot}\right) = 4\log\left(\frac{\sigma_{\rm los}}{\rm km\ s^{-1}}\right) + 1.96^{+0.05}_{-0.06}, \tag{7}$$

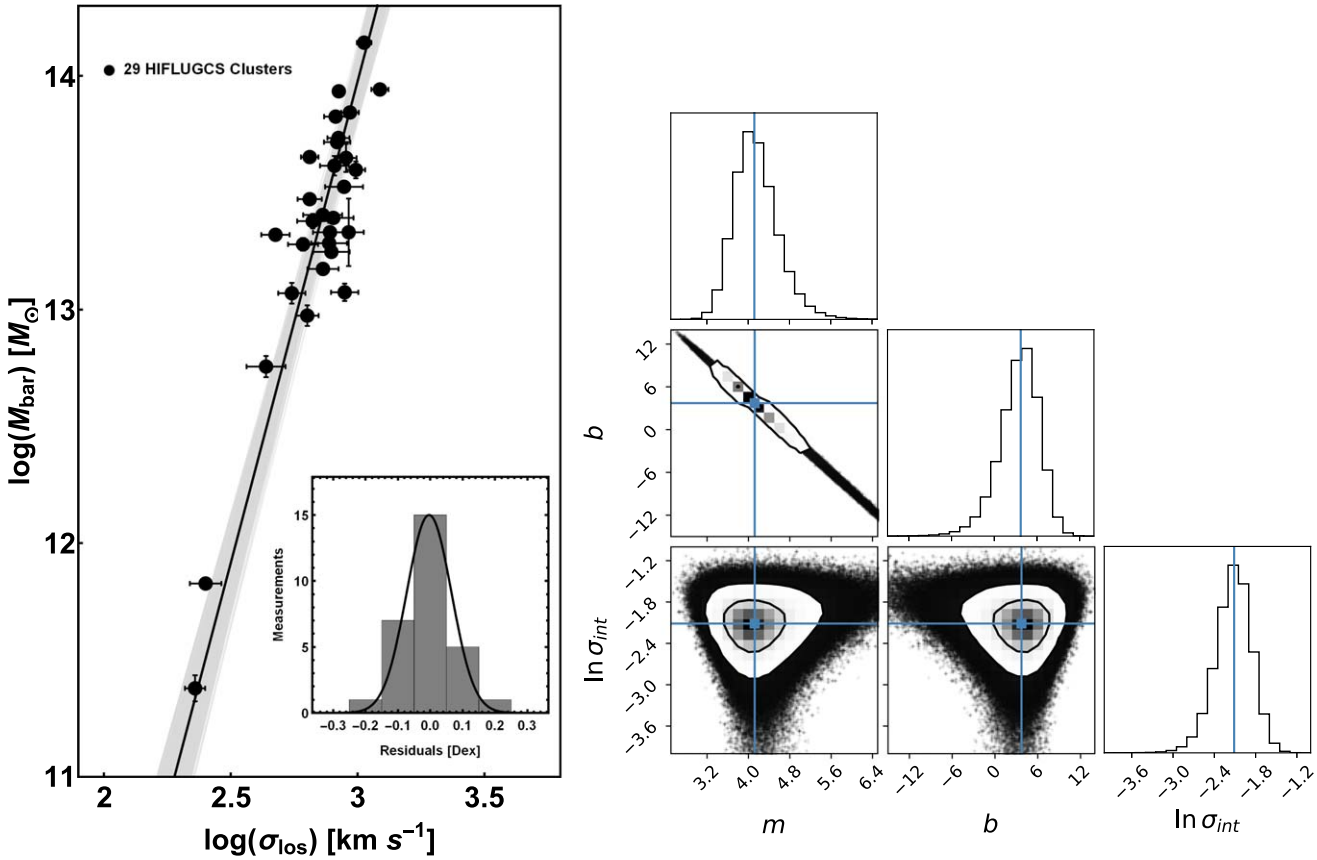

Figure 2. The MVDR in 29 HIFLUGCS galaxy clusters. Left panel: the kinematic scale relation between the baryonic mass $M_{\rm bar}$ and the flat los velocity dispersion $\sigma_{\rm los}$ of member galaxies. The black line represents the best-fitting relation found with MCMC, $\log(M_{\rm bar}/M_\odot) = 4.1^{+0.4}_{-0.4}\log(\sigma_{\rm los}/{\rm km\ s^{-1}}) + 1.6^{+1.0}_{-1.3}$. The gray shaded area represents the one-sigma region around the best-fitting black solid line. The inset panel is a histogram of the orthogonal residuals presenting as a Gaussian distribution. Right panel: constraints on the regression parameters for the MVDR with marginalized one-dimensional (histograms) and two-dimensional posterior distributions.

which is still tight with the lognormal intrinsic scatter of $12^{+3}_{-3}\%$. The uncertainty of the intercept is dramatically reduced for the fixed slope. The reason is that the degeneracy in the m–b diagram is broken.

Without the correction with the stellar mass, we also study the scaling relation of $M_{\rm gas}$ and $\sigma_{\rm los}$ by the ODR MCMC method, which gives

$$\log\left(\frac{M_{\rm gas}}{M_\odot}\right) = 4.3^{+0.5}_{-0.4}\log\left(\frac{\sigma_{\rm los}}{\rm km\ s^{-1}}\right) + 1.0^{+1.1}_{-1.3}. \quad (8)$$

Although $f_{\rm star}$ is relatively large for the two smallest clusters, the resulting difference in the slope changes from 4.1 to 4.3. Moreover, the relation is still tight with the lognormal intrinsic scatter of $12^{+3}_{-3}\%$.

Two low-mass clusters dominate the slope and the intercept. Excluding these two points, we get a different MVDR with a larger scatter: $m = 5.4^{+2.2}_{-1.1}$ and $b = -2.0^{+3.2}_{-6.3}$. This finding is analogous to the important influence of low surface brightness disks to the BTFR: smaller galaxy clusters play a major role in the MVDR.

Although the flat velocity dispersion is more representative of the total kinetic energy, we still check the MVDR with the velocity dispersion measured at r_{500} attributed to the baryonic masses estimated within r_{500}. This makes a difference, as the velocity dispersion profiles in half of the sample have not flattened yet at r_{500}. It yields a slightly steeper MVDR: $m = 4.5^{+0.5}_{-0.4}$ and $b = 0.6^{+1.1}_{-1.4}$.

3.2. Residuals

We present the orthogonal residuals by considering Δ_i in Equation (4) with m and b in Equation (6) versus four cluster quantities: virial temperature $kT_{\rm vir}$, cluster radius r_{500}, baryonic mass surface density $\Sigma_{\rm bar}$, and redshift; see Figure 3. The tiny residuals range between -0.2 and 0.2 and display no significant correlation with the four cluster properties. These properties are reminiscent of the BTFR for individual galaxies.

4. Discussions

4.1. Implications of the CLASH RAR

Tian et al. (2020) have revealed a tight RAR shown by 20 CLASH BCGs and clusters as $g_{\rm obs} \simeq \sqrt{g_{\rm bar} g_\ddagger}$. If we related $g_{\rm obs}(r)$ to the velocity dispersion as $g_{\rm obs}(r) = J(r)^{1/2}\sigma^2_{\rm r,3D}/r$ and input $g_{\rm bar}(r) = GM_{\rm bar}(<r)/r^2$ into the CLASH RAR, we can recover the MVDR: $M_{\rm bar} = \sigma^4_{r,3D}J(r)G^{-1}g_\ddagger^{-1}$. Here, the Jeans factor $J(r)$ is related to the density profile and the anisotropic parameter β by the Jeans equation (e.g., see Milgrom 1984; Sanders 2010; Famaey & McGaugh 2012):

$$-[J(\tilde{r})]^{1/2} = \frac{d\ln\tilde{\rho}}{d\ln\tilde{r}} + 2\beta, \quad (9)$$

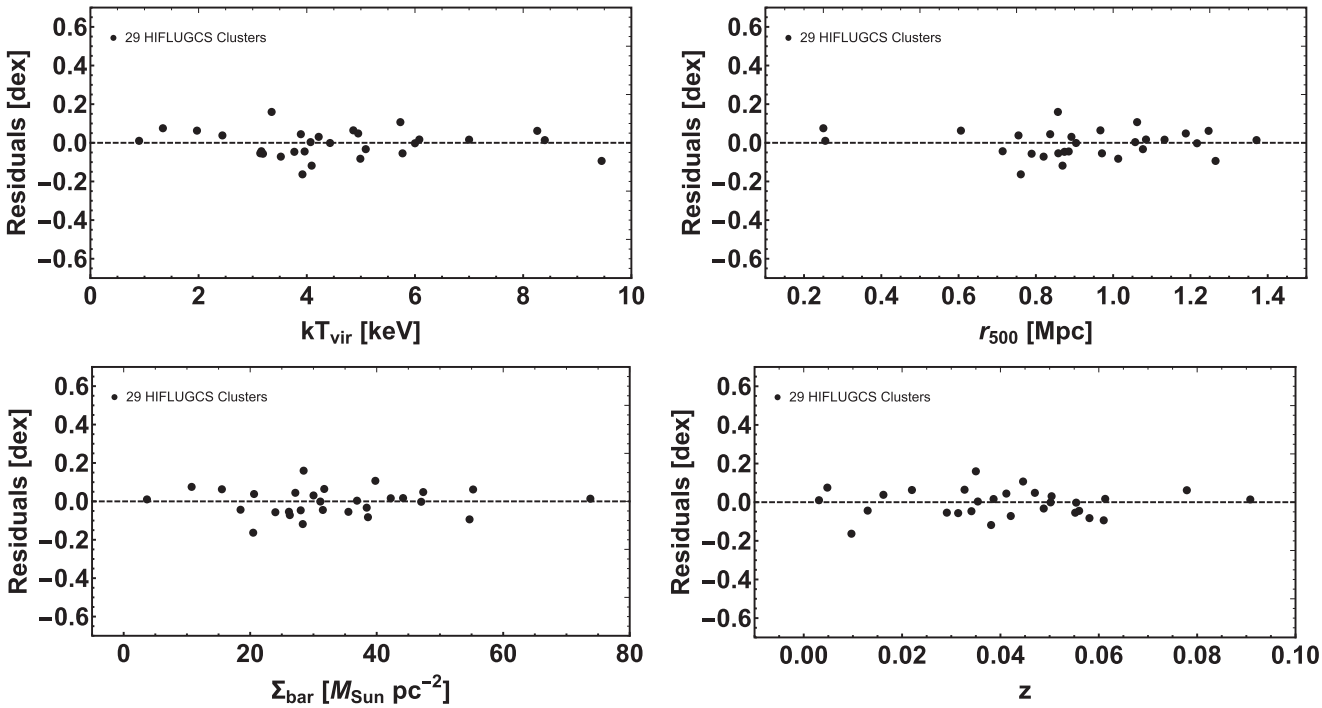

Figure 3. The residuals of the MVDR in 29 HIFLUGCS clusters. The orthogonal residuals after subtracting Equation (6) against four cluster properties: virial temperature kT_{vir} (upper left), cluster radius r_{500} (upper right), baryonic mass surface density Σ_{bar} (lower left), and redshift (lower right). The dashed line represents zero difference.

where $\tilde{r} \equiv r/r_\ddagger$ and $\tilde{\rho} \equiv \rho/\rho_\ddagger$ with the scale length $r_\ddagger = \sigma^2_{r,3D} g_\ddagger^{-1}$ and the scale density $\rho_\ddagger = \sigma^4_{r,3D}(4\pi r_\ddagger^3 G g_\ddagger)^{-1}$. Therefore, as $\tilde{r} \to \infty$, we have $J(\tilde{r}) \to J_\infty$ and $d\ln\tilde{\rho}/d\ln\tilde{r} \to -\alpha_\infty$, which leads to $J_\infty = (\alpha_\infty - 2\beta)^2$.

By the implications of the CLASH RAR, the MVDR is presented as

$$\log(M_{bar}) = 4\log(\sigma_{r,3D}) + \log(J_\infty G^{-1} g_\ddagger^{-1}). \quad (10)$$

Here, the factor α_∞ depends on the density profile of the systems, and $\beta = 0$ for isotropic case. Thus, the intercept involves J_∞, the new acceleration scale $g_\ddagger$, and the gravitational constant G.

For a special case of the isotropic parameter $\beta = 0$ and the flat velocity dispersion $\sigma_{r,3D} = \text{const.}$, the radial velocity dispersion in the three-dimensional $\sigma_{r,3D}$ in Equation (10) is identical to the flat los velocity dispersion σ_{los}. To estimate σ_{los} from $\sigma_{r,3D}$, we consider the surface density at the projected radius weighted σ (e.g., see chapter 4.2 in Binney & Tremaine 2008). Thus, it is trivial to show that $\sigma_{los} = \sigma_{r,3D}$ for this special case.

The two unknown factors, $g_\ddagger$ and J_∞ in Equation (10), can be estimated by the intercept of Equation (7). For example, if we take $\alpha_\infty \in [3, 5]$ and $\beta = 0$, then the corresponding Jeans factor $J_\infty \in [9, 25]$. From the intercept, we estimate the new acceleration scale $g_\ddagger = (0.8 - 2.2) \times 10^{-9}\,\mathrm{m\,s^{-2}}$, which is about ten times larger than $g_\dagger$. The actual value of $g_\ddagger$ requires the precise measurement of $\langle J_\infty \rangle$ of the sample. However, we can estimate the Jeans factor by adopting the new acceleration scale in the CLASH RAR, $g_\ddagger = (2.0 \pm 0.1) \times 10^{-9}\,\mathrm{m\,s^{-2}}$. Comparing with Equation (7) again, we get $\langle J_\infty \rangle = 23.7 \pm 1.4$, and then $\langle \alpha_\infty - 2\beta \rangle = 4.86 \pm 0.14$.

In our calculation, we require the radius r to be far away from the scale length $r_\ddagger$ to justify the asymptotic behavior of the Jeans factor $J(\tilde{r}) \to J_\infty$. With the new acceleration scale $g_\ddagger = 1.4 \times 10^{-9}\,\mathrm{m\,s^{-2}}$, we can estimate $r_\ddagger = \sigma^2_{last} g_\ddagger^{-1}$ in 29 HIFLUGCS clusters (see the scale parameters in Milgrom 1984). Therefore, we get the average of $\langle r_\ddagger \rangle = 14$ kpc, which is insignificant compared to the average radius of last binned data in Table 2, $\langle r_{last} \rangle \approx 1300$ kpc. This result is in good agreement with our previous assumption of $r \gg r_\ddagger$.

4.2. Test For the Dark Matter Model

An MVDR can be derived from ΛCDM under general considerations. Following Mo et al. (1998), Navarro & Steinmetz (2000), McGaugh et al. (2010), and McGaugh (2012), we compare the MVDR to that expected in the ΛCDM model. The enclosed total mass within this radius is given by

$$M_{500} = \frac{4\pi}{3}(500\rho_{crit}) r_{500}^3, \quad (11)$$

where $\rho_{crit} = 3H_0^2/8\pi G$ is the critical density of the universe.

To relate the dark matter mass with velocity dispersion, we consider the gravitational potential traced by the velocity dispersion in pressure-supported systems as

$$\frac{GM_{500}}{r_{500}^2} = \frac{J^{1/2}(r)\sigma^2_{r,3D}}{r_{500}}. \quad (12)$$

Together with the baryon fraction $f_{bar} = M_{bar}/M_{500}$ at r_{500}, we derive the relation between the baryonic mass and the velocity dispersion in ΛCDM

$$\log(M_{bar}) = 3\log(\sigma_{los}) + \log\left(\frac{\sqrt{2}\,J^{3/4} f_{bar}}{\sqrt{500}\,GH_0}\right). \quad (13)$$

Here, with the flat velocity dispersion and the assumption of the isotropic parameter, we adopt $\sigma_{los} = \sigma_{r,3D}$. Noticeably, the

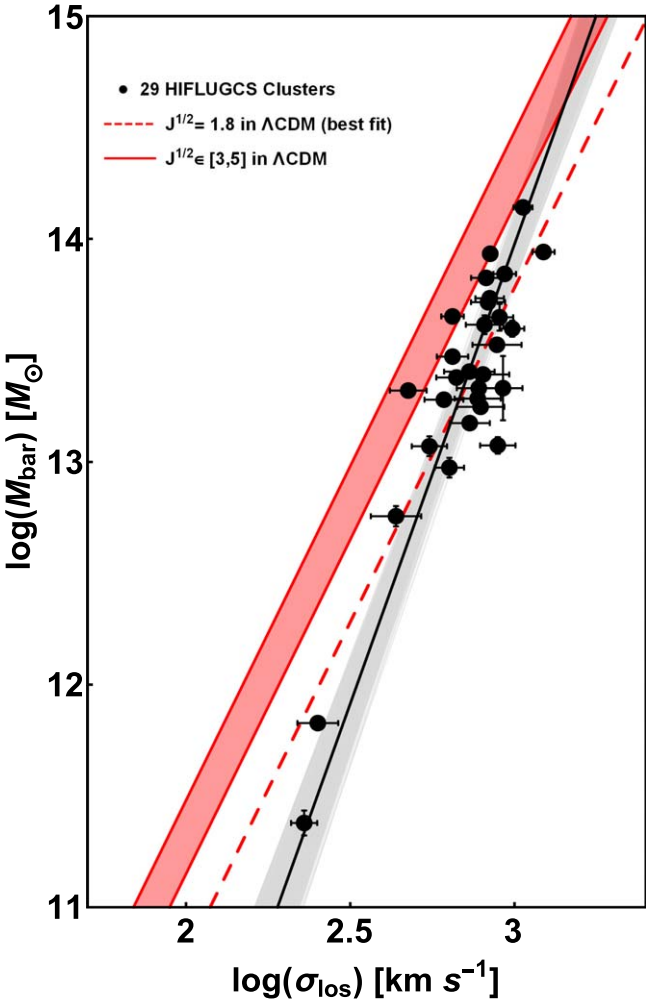

Figure 4. Test for the dark matter model. Black solid circles, black solid line, and gray shaded area are the same as in Figure 2. The red area and dashed line show the ΛCDM prediction with the choice of $J^{1/2} \in [3, 5]$ and the best-fit of $J^{1/2} = 1.8$, respectively.

ΛCDM model predicts a slope of three, which does not agree with the observed value of four.

The examination of the dark matter model requires the estimation of all of the parameters of the intercept in Equation (12): a Hubble constant, the baryon fraction, and the Jeans factor. At r_{500}, we adopt $f_{bar} = 0.13$ as measured by Donahue et al. (2014) and Tian et al. (2020). While the Jeans factor depends on the density profile, we assume a possible range of $J^{1/2} \in [3, 5]$. A red region in Figure 4 shows the corresponding relation. The ΛCDM prediction is systematically higher than the empirical MVDR, despite adopting a baryon fraction that is lower than the cosmic value.

To understand the best value of the Jeans factor, we implement the ODR MCMC technique for 29 HIFLUGCS clusters with the fixed slope ($m = 3$), which gives

$$\log\left(\frac{M_{bar}}{M_\odot}\right) = 3\log\left(\frac{\sigma_{los}}{\text{km s}^{-1}}\right) + 4.78^{+0.05}_{-0.06}. \quad (14)$$

The intercept gives the best fit of $J^{1/2} = 1.8$, shown as the red dashed line in Figure 4. In this case, the velocity dispersion needs to be close to the circular velocity, which it is manifestly not. As the best-fit Jeans factor is significantly lower than is plausible, it reveals a fine-tuning problem as discussed in the next section.

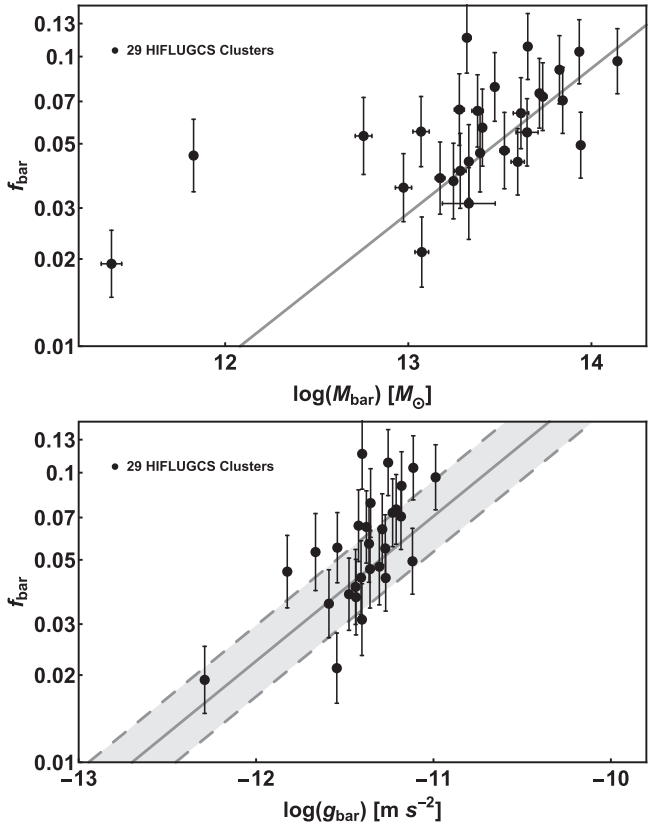

Figure 5. The baryonic factions of the 29 HIFLUGCs Clusters (black solid circles) and those implied by the CLASH RAR (gray solid lines) are plotted against baryonic mass M_{bar} (upper panel) and baryonic acceleration g_{bar} (lower panel). The dashed lines and the gray region are from the standard deviation of r_{500}.

In the literature, Mo et al. (1998) predicted the dynamical MVDR in the dark matter model as $M_{200} \propto V_{200}^3$. Moreover, from both simulations and analytical relations, the results indicated $M_{200} \propto \sigma^3$ (Evrard et al. 2008; Rines et al. 2013). To relate the dynamical mass M_{200} with the baryonic mass M_{bar} requires a specific model of the baryon faction. If the baryon faction is a constant for all of the clusters, the dark matter prediction is inconsistent with the observed slope of four.

Observational results that obtain a slope close to three cover only a small dynamic range in mass. Most studies of clusters only cover the range $10^{14}\,M_\odot < M_{200} < 10^{15}\,M_\odot$, and their results have not been tested for $M_{200} < 10^{13}\,M_\odot$. Since our sample covers a larger range in mass, it provides a better constraint on the slope. Given the small number of groups with $M_{bar} < 10^{12}\,M_\odot$, further study will be important.

4.3. Implications for the Baryon Fraction

In this section, we study the baryon fraction $f_{bar} \equiv M_{bar}/M_{obs} = g_{bar}/g_{obs}$ of the 29 clusters. We estimate $f_{bar}(r_{500})$ by considering the observational acceleration as $g_{obs}(r_{500}) = J_\infty^{1/2}\sigma_{last}^2/r_{500}$. We consider $\sigma_{last} \simeq \sigma_{500}$, given the flat velocity dispersion. In addition, we adopt $J_\infty^{1/2} = 4 \pm 1$. The precise value of J_∞ should vary among the sample, inducing scatter. The derived f_{bar} values are plotted against baryonic mass (upper panel) and baryonic acceleration (lower panel) in Figure 5.

For comparison, the CLASH RAR (Tian et al. 2020) implies

$$f_{\rm bar}(r) \approx \sqrt{g_{\rm bar}(r)/g_{\ddagger}}. \quad (15)$$

Here, we estimate the baryonic acceleration at r_{500} by $g_{\rm bar}(r_{500}) = GM_{\rm bar}(<r_{500})/r_{500}^2$. Since r_{500} varies in every HIFLUGCS cluster, it contributes to the scatter of the relation. We demonstrate Equation (15) with the mean $\langle r_{500}\rangle = 917$ kpc and error propagation to $g_{\rm bar}(r_{500})$ from the standard deviation of $\sigma_{r_{500}} = 259$ kpc; see gray solid and dashed line in Figure 5. To compare with Equation (15), we assume $g_{\ddagger} = 2.0 \times 10^{-9}\,{\rm m\,s^{-2}}$ as found in Tian et al. (2020).

The 29 HIFLUGCS clusters are consistent with the implication of the CLASH RAR in Figure 5. The relation of the baryon fraction with acceleration is reminiscent of MOND-like behavior ($f_{\rm bar} \propto g_{\rm bar}^{1/2}$), albeit with a different acceleration scale than in galaxies (McGaugh 2004, 2015; Milgrom 2020).

5. Summary

In this paper, we investigate the correlation between the baryonic mass of 29 HIFLUGCS clusters and the flat velocity dispersion of their member galaxies. We have calculated the baryonic mass by combining the X-ray gas mass (Zhang et al. 2011) and the stellar mass correction from Giodini et al. (2009). By spatially resolving the velocity dispersion profiles, we find a flat velocity dispersion at large radii. The resulting MVDR is well described by a power-law relation, $M_{\rm bar} \propto \sigma_{\rm los}^{4.1\pm0.4}$, with a lognormal intrinsic scatter of 12^{+3}_{-3}%. This is consistent with the implication of the CLASH RAR, $g_{\rm obs} \simeq \sqrt{g_{\rm bar}\, g_{\ddagger}}$. Furthermore, the residuals do not correlate with other cluster properties such as temperature, cluster radius r_{500}, baryonic surface density, and redshift.

The MVDR can be naturally explained in the MOND paradigm. The slope of four is a prediction of MOND. However, the intercept of the MVDR indicates an acceleration scale $g_{\ddagger}$ that is larger than that in galaxies. Why clusters should exhibit MOND-like behavior with a shifted acceleration scale is a mystery in any theory. In pure MOND, there should be no shift. In terms of dark matter, there is no reason to expect MOND-like behavior at all. One conceivable explanation is a dependence of the action on the depth of the potential well in addition to the acceleration (Zhao & Famaey 2012).

In this paper, we have derived the expected MVDR in ΛCDM from general considerations and examined the baryon fraction in our sample. We find that ΛCDM gives an MVDR with a slope of three, when we assume the Jeans factor and the baryon fraction are independent of the baryonic mass. This is in serious tension with the observed slope of four. Furthermore, the predicted intercept of the MVDR is systematically higher than is observed. This indicates a residual mass problem in ΛCDM: the predicted baryonic masses of galaxy clusters are more than that required by the observed kinematics. Possibly, this discrepancy could be compensated for by introducing a systematic dependence of the Jeans factor and the baryon fraction on the baryonic mass of the clusters, but this creates a fine-tuning problem to get the slope right without inducing too much scatter.

We have revealed a tight MVDR on the cluster scale. To explore the full range of this relation requires more data from smaller galaxy clusters. This is also imperative for the understanding of the CLASH RAR in the small acceleration regime.

We thank M. Milgrom for many inspiring discussions on this work, and the anonymous referee for the valuable comments to improve the clarity of this paper. Y.T. and C.M.K. are supported by the Taiwan Ministry of Science and Technology grant MOST 108-2112-M-008-006 and MOST 109-2112-M-008-005. P.C.Y. is supported by the Taiwan Ministry of Science and Technology grant MOST 109-2112-M-155-001. S. S.M. and P.L. are supported in part by NASA ADAP grant 80NSSC19k0570 and NSF PHY-1911909.

ORCID iDs

Yong Tian https://orcid.org/0000-0001-9962-1816
Po-Chieh Yu https://orcid.org/0000-0001-8894-0854
Pengfei Li https://orcid.org/0000-0002-6707-2581
Stacy S. McGaugh https://orcid.org/0000-0002-9762-0980
Chung-Ming Ko https://orcid.org/0000-0002-6459-4763

References

Agulli, I., Aguerri, J. A. L., Sánchez-Janssen, R., et al. 2016, MNRAS, 458, 1590
Angus, G. W., Famaey, B., & Buote, D. A. 2008, MNRAS, 387, 1470
Aquino-Ortíz, E., Valenzuela, O., Sánchez, S. F., et al. 2018, MNRAS, 479, 2133
Arnold, T. J., Martini, P., Mulchaey, J. S., Berti, A., & Jeltema, T. E. 2009, ApJ, 707, 1691
Bahcall, N. A. 1977, ARA&A, 15, 505
Bai, L., Rieke, G. H., Rieke, M. J., Christlein, D., & Zabludoff, A. I. 2009, ApJ, 693, 1840
Barat, D., D'Eugenio, F., Colless, M., et al. 2019, MNRAS, 487, 2924
Beers, T. C., Flynn, K., & Gebhardt, K. 1990, AJ, 100, 32
Binney, J., & Tremaine, S. 2008, Galactic Dynamics: Second Edition (Princeton, NJ: Princeton Univ. Press)
Böhringer, H., Schuecker, P., Guzzo, L., et al. 2004, A&A, 425, 367
Böhringer, H., Voges, W., Huchra, J. P., et al. 2000, ApJS, 129, 435
Cappellari, M., McDermid, R. M., Alatalo, K., et al. 2013, MNRAS, 432, 1862
Catinella, B., Kauffmann, G., Schiminovich, D., et al. 2012, MNRAS, 420, 1959
Cava, A., Bettoni, D., Poggianti, B. M., et al. 2009, A&A, 495, 707
Chae, K.-H., Bernardi, M., Sheth, R. K., & Gong, I.-T. 2019, ApJ, 877, 18
Chan, M. H., & Del Popolo, A. 2020, MNRAS, 492, 5865
Chiboucas, K., & Mateo, M. 2006, AJ, 132, 347
Chilingarian, I., Cayatte, V., Revaz, Y., et al. 2009, Sci, 326, 1379
Chilingarian, I. V., Cayatte, V., Durret, F., et al. 2008, A&A, 486, 85
Chiu, I., Mohr, J. J., McDonald, M., et al. 2018, MNRAS, 478, 3072
Coziol, R., Andernach, H., Caretta, C. A., Alamo-Martínez, K. A., & Tago, E. 2009, AJ, 137, 4795
Dehghan, S., Johnston-Hollitt, M., Colless, M., & Miller, R. 2017, MNRAS, 468, 2645
Desmond, H., & Wechsler, R. H. 2015, MNRAS, 454, 322
Desmond, H., & Wechsler, R. H. 2017, MNRAS, 465, 820
Donahue, M., Voit, G. M., Mahdavi, A., et al. 2014, ApJ, 794, 136
Dutton, A. A., Conroy, C., van den Bosch, F. C., Prada, F., & More, S. 2010, MNRAS, 407, 2
Ebeling, H., Edge, A. C., Bohringer, H., et al. 1998, MNRAS, 301, 881
Ettori, S., Tozzi, P., Borgani, S., & Rosati, P. 2004, A&A, 417, 13
Evrard, A. E., Bialek, J., Busha, M., et al. 2008, ApJ, 672, 122
Faber, S. M., & Jackson, R. E. 1976, ApJ, 204, 668
Faber, S. M., Wegner, G., Burstein, D., et al. 1989, ApJS, 69, 763
Famaey, B., & McGaugh, S. S. 2012, LRR, 15, 10
Ferguson, H. C. 1989, AJ, 98, 367
Ferguson, H. C., & Sandage, A. 1990, AJ, 100, 1
Fogarty, L. M. R., Scott, N., Owers, M. S., et al. 2015, MNRAS, 454, 2050
Foreman-Mackey, D., Farr, W., Sinha, M., et al. 2019, JOSS, 4, 1864
Foreman-Mackey, D., Hogg, D. W., Lang, D., & Goodman, J. 2013, PASP, 125, 306
Giodini, S., Pierini, D., Finoguenov, A., et al. 2009, ApJ, 703, 982
Guzzo, L., Schuecker, P., Böhringer, H., et al. 2009, A&A, 499, 357
Hoffer, A. S., Donahue, M., Hicks, A., & Barthelemy, R. S. 2012, ApJS, 199, 23
Hudson, D. S., Mittal, R., Reiprich, T. H., et al. 2010, A&A, 513, A37

Hudson, M. J., Lucey, J. R., Smith, R. J., Schlegel, D. J., & Davies, R. L. 2001, MNRAS, 327, 265
Jones, C., & Forman, W. 1984, ApJ, 276, 38
Jørgensen, I., Chiboucas, K., Webb, K., & Woodrum, C. 2018, AJ, 156, 224
Katz, H., Desmond, H., McGaugh, S., & Lelli, F. 2019, MNRAS, 483, L98
Kilborn, V. A., Forbes, D. A., Barnes, D. G., et al. 2009, MNRAS, 400, 1962
Kneib, J.-P., & Natarajan, P. 2011, A&ARv, 19, 47
Kravtsov, A. V., & Borgani, S. 2012, ARA&A, 50, 353
Laine, S., van der Marel, R. P., Lauer, T. R., et al. 2003, AJ, 125, 478
Lauer, T. R., Postman, M., Strauss, M. A., Graves, G. J., & Chisari, N. E. 2014, ApJ, 797, 82
Lea, S. M., Silk, J., Kellogg, E., & Murray, S. 1973, ApJL, 184, L105
Lee, G.-H., Hwang, H. S., Lee, M. G., et al. 2015, ApJ, 800, 80
Lelli, F., McGaugh, S. S., & Schombert, J. M. 2016, ApJL, 816, L14
Lelli, F., McGaugh, S. S., Schombert, J. M., Desmond, H., & Katz, H. 2019, MNRAS, 484, 3267
Lelli, F., McGaugh, S. S., Schombert, J. M., & Pawlowski, M. S. 2017, ApJ, 836, 152
Li, P., Lelli, F., McGaugh, S., & Schombert, J. 2018, A&A, 615, A3
Lin, Y.-T., & Mohr, J. J. 2004, ApJ, 617, 879
Liu, S.-F., Yuan, Q.-R., Yang, Y.-B., et al. 2011, AJ, 141, 99
Mahdavi, A., & Geller, M. J. 2001, ApJL, 554, L129
Marziani, P., D'Onofrio, M., Bettoni, D., et al. 2017, A&A, 599, A83
McGaugh, S. S. 2004, ApJ, 609, 652
McGaugh, S. S. 2011, PhRvL, 106, 121303
McGaugh, S. S. 2012, AJ, 143, 40
McGaugh, S. S. 2015, CaJPh, 93, 250
McGaugh, S. S., Lelli, F., & Schombert, J. M. 2016, PhRvL, 117, 201101
McGaugh, S. S., Li, P., Lelli, F., & Schombert, J. M. 2018, NatAs, 2, 924
McGaugh, S. S., Schombert, J. M., Bothun, G. D., & de Blok, W. J. G. 2000, ApJL, 533, L99
McGaugh, S. S., Schombert, J. M., de Blok, W. J. G., & Zagursky, M. J. 2010, ApJL, 708, L14
Milgrom, M. 1983, ApJ, 270, 365
Milgrom, M. 1984, ApJ, 287, 571
Milgrom, M. 2019, PhRvD, 99, 044041
Milgrom, M. 2020, SHPMP, 71, 170
Misgeld, I., Mieske, S., & Hilker, M. 2008, A&A, 486, 697
Misgeld, I., Mieske, S., Hilker, M., et al. 2011, A&A, 531, A4
Mo, H. J., Mao, S., & White, S. D. M. 1998, MNRAS, 295, 319
Mulchaey, J. S., & Zabludoff, A. I. 1998, ApJ, 496, 73
Navarro, J. F., & Steinmetz, M. 2000, ApJ, 538, 477
Overzier, R. A. 2016, A&ARv, 24, 14
Owers, M. S., Nulsen, P. E. J., & Couch, W. J. 2011, ApJ, 741, 122
Park, H. S., Lee, M. G., Hwang, H. S., et al. 2010, ApJ, 709, 377
Poggianti, B. M., Fasano, G., Omizzolo, A., et al. 2016, AJ, 151, 78
Pointecouteau, E., & Silk, J. 2005, MNRAS, 364, 654
Popesso, P., Biviano, A., Böhringer, H., Romaniello, M., & Voges, W. 2005, A&A, 433, 431
Postman, M., Coe, D., Benítez, N., et al. 2012, ApJS, 199, 25
Rafferty, D. A., McNamara, B. R., & Nulsen, P. E. J. 2008, ApJ, 687, 899
Reiprich, T. H., & Böhringer, H. 2002, ApJ, 567, 716
Rines, K., Geller, M. J., Diaferio, A., & Kurtz, M. J. 2013, ApJ, 767, 15
Rines, K. J., Geller, M. J., Diaferio, A., & Hwang, H. S. 2016, ApJ, 819, 63
Rong, Y., Li, H., Wang, J., et al. 2018, MNRAS, 477, 230
Sakai, S., Kennicutt, Robert, C., & Moss, C, J. 2012, ApJS, 199, 36
Sanders, R. H. 1994, A&A, 284, L31
Sanders, R. H. 1999, ApJL, 512, L23
Sanders, R. H. 2003, MNRAS, 342, 901
Sanders, R. H. 2010, MNRAS, 407, 1128
Sanders, R. H., & McGaugh, S. S. 2002, ARA&A, 40, 263
Schneider, D. P., Gunn, J. E., & Hoessel, J. G. 1983, ApJ, 268, 476
Schombert, J. M. 1986, ApJS, 60, 603
Schuberth, Y., Richtler, T., Dirsch, B., et al. 2006, A&A, 459, 391
Smith, R. J., Hudson, M. J., Nelan, J. E., et al. 2004, AJ, 128, 1558
Smith, R. J., Lucey, J. R., Hudson, M. J., Schlegel, D. J., & Davies, R. L. 2000, MNRAS, 313, 469
Smith, R. J., Lucey, J. R., Schlegel, D. J., et al. 2001, MNRAS, 327, 249
Sohn, J., Geller, M. J., Zahid, H. J., et al. 2017, ApJS, 229, 20
Szabo, T., Pierpaoli, E., Dong, F., Pipino, A., & Gunn, J. 2011, ApJ, 736, 21
Thomas, C. F., Moss, C., James, P. A., et al. 2008, A&A, 486, 755
Tian, J.-T., Yuan, Q.-R., Zhou, X., et al. 2012, RAA, 12, 1381
Tian, Y., & Ko, C.-M. 2017, MNRAS, 472, 765
Tian, Y., & Ko, C.-M. 2019, MNRAS, 488, L41
Tian, Y., Umetsu, K., Ko, C.-M., Donahue, M., & Chiu, I. N. 2020, ApJ, 896, 70
Tully, R. B., & Fisher, J. R. 1977, A&A, 500, 105
Tyler, K. D., Rieke, G. H., & Bai, L. 2013, ApJ, 773, 86
Umetsu, K. 2020, A&ARv, 28, 7
Umetsu, K., Medezinski, E., Nonino, M., et al. 2014, ApJ, 795, 163
Umetsu, K., Zitrin, A., Gruen, D., et al. 2016, ApJ, 821, 116
Verheijen, M. A. W. 2001, ApJ, 563, 694
Von Der Linden, A., Best, P. N., Kauffmann, G., & White, S. D. M. 2007, MNRAS, 379, 867
Wechsler, R. H., & Tinker, J. L. 2018, ARA&A, 56, 435
Wenger, M., Ochsenbein, F., Egret, D., et al. 2000, A&AS, 143, 9
Xue, Y.-J., & Wu, X.-P. 2000, ApJ, 538, 65
Zhang, Y. Y., Andernach, H., Caretta, C. A., et al. 2011, A&A, 526, A105
Zhao, H., & Famaey, B. 2012, PhRvD, 86, 067301
Zitrin, A., Bartelmann, M., Umetsu, K., Oguri, M., & Broadhurst, T. 2012, MNRAS, 426, 2944
Zwicky, F. 1933, AcHPh, 6, 110